Prepared for the
NATIONAL AERONAUTICS AND SPACE ADMINISTRATION

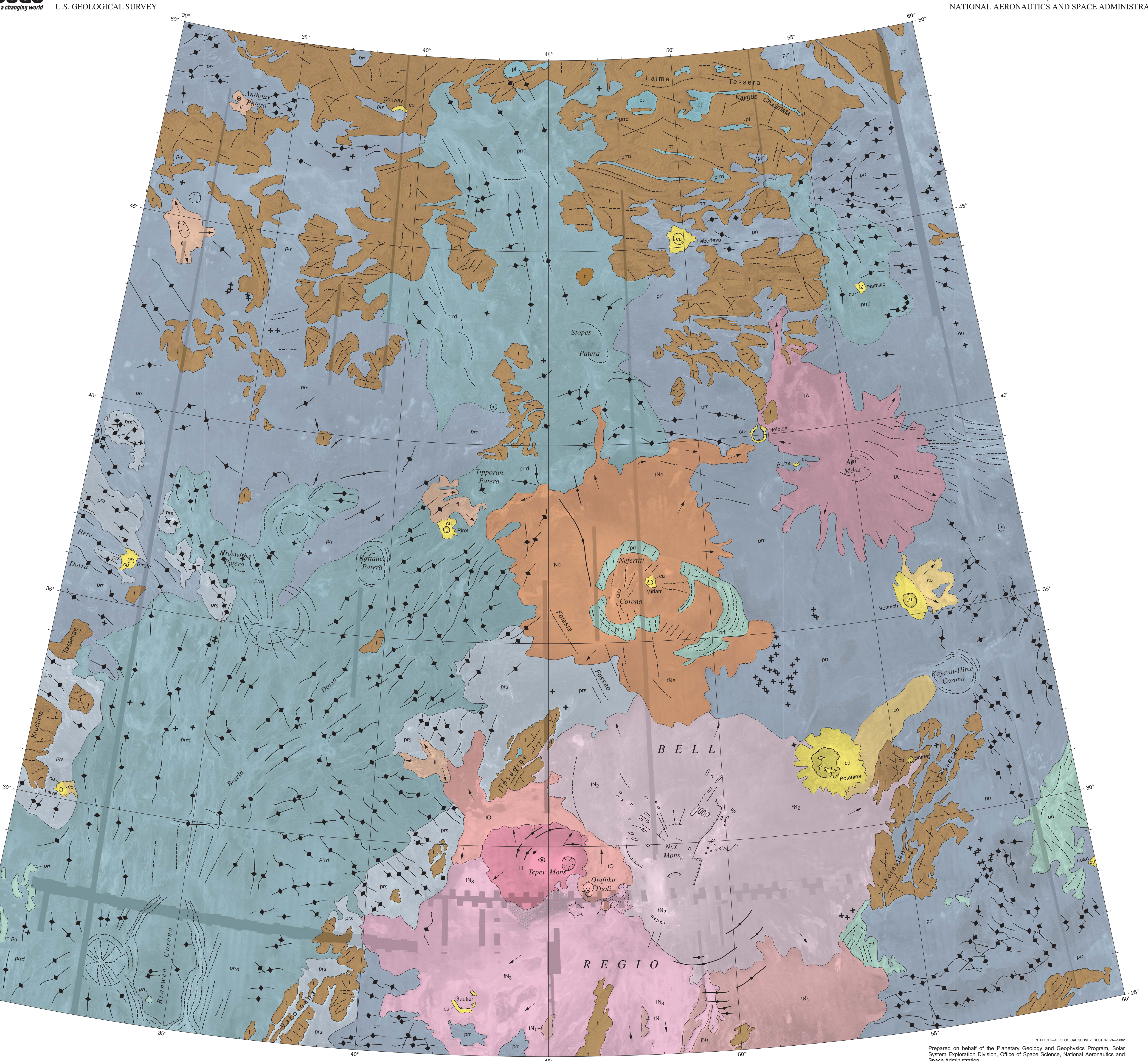

INTERIOR—GEOLOGICAL SURVEY, RESTON, VA—2002

Prepared on behalf of the Planetary Geology and Geophysics Program, Solar System Exploration Division, Office of Space Science, National Aeronautics and Space Administration
Edited by Derrick D. Hirsch; cartography by Hugh F. Thomas and Darlene A. Ryan
Manuscript approved for publication March 14, 2001

SCALE 1:4 711 886 (1 mm = 4.712 km) AT 25° LATITUDE
1:5 000 000 AT 34° AND 73° LATITUDES
LAMBERT PROJECTION

CORRELATION OF MAP UNITS

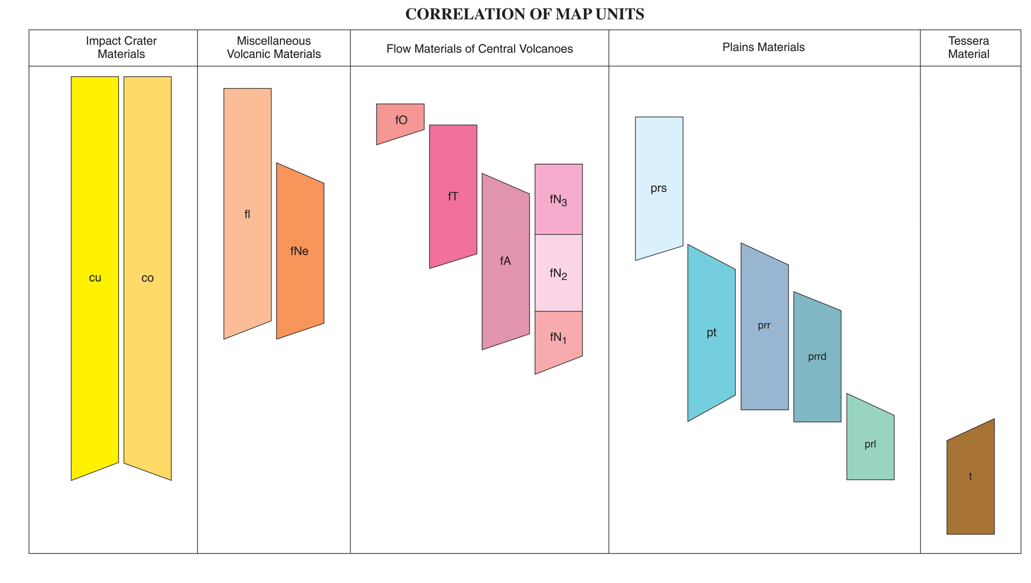

DESCRIPTION OF MAP UNITS

FLOW MATERIALS OF CENTRAL VOLCANOES

fO **Lobate material of Otafuku Tholi**—Radar-bright lobate deposits encircling portions of Tepev Mons and superposed on units fN$_2$ and fT. Embays portions of the tessera to the north. *Interpretation*: Lava flows from the north edifice of Otafuku Tholi. Radar brightness in the largest lobate unit consistent with terrestrial aa morphology

fT **Lobate material of Tepev Mons**—Narrow interfingered radar-bright and dark lobes which form an apron around Tepev Mons; lobes radiate ~200 km from the summit of the edifice; no clear contact between these flows and materials of Nyx Mons. *Interpretation*: Lava flows erupted from the Tepev Mons calderas, nearby pit craters and fissures

fA **Lobate material of Api Mons**—Lobate deposits which emanate from a central complex of small domes, pit craters, and annular fractures near the summit of Api Mons; typically of low radar return, but some lobes are moderately radar bright; embays Laima Tessera to the north and superposes regional plains units. *Interpretation*: Lava flows associated with eruptions from the summit area of Api Mons

fN$_3$ **Upper lobate material of Nyx Mons**—Complex of lobate-margined deposits; typically radial to Nyx Mons; superposes radar-dark material of units fN$_1$ and fN$_2$. Radar brightness varies from moderate to very bright. *Interpretation*: Lava flows from a variety of source vents that post-date the materials of units fN$_1$ and fN$_2$

fN$_2$ **Middle lobate material of Nyx Mons**—Low radar return, generally homogeneous lobate or scalloped deposits; typically radial to Nyx Mons; isolated bright lobate margins east of Nyx summit. *Interpretation*: Lava flows from Nyx Mons which post-date the fN$_1$ flows. The isolated margins may represent the transition of smooth, broad lava flows to rougher, more distinct lobate structures; these lobes may also be higher-standing, embayed materials of unit fN$_1$

fN$_1$ **Lower lobate material of Nyx Mons**—Low-moderate radar return lobate deposits radial to Nyx Mons; superpose regional plains and tesserae to the south. *Interpretation*: Lava flows from Nyx Mons that predate other shield-forming units in this region. Backscatter coefficients are consistent with terrestrial smooth pahoehoe flows

MISCELLANEOUS VOLCANIC MATERIALS

fl **Localized lobate material**—Lobate deposits radiating from a central depression or low-relief dome in the plains; typically less than 100 km in radial extent; variable radar brightness with digitate narrow lobes common. *Interpretation*: Lava flows associated with small shield volcanoes and calderas in the plains

fNe **Lobate material of Nefertiti Corona**—Lobate deposits radial to Nefertiti Corona; superpose the prrd and prr plains units, but no clear stratigraphic relationship with deposits of Nyx Mons or Tepev Mons; typically of low radar brightness. *Interpretation*: Lava flows associated with the post Mons uplift stage of corona formation

PLAINS MATERIALS

prs **Smooth plains material**—Homogeneous radar image texture, typically of lower radar brightness at ~40° incidence angle than any other map unit; wrinkle ridges are typically subdued but of similar orientation to those of nearby densely ridged plains; contacts between smooth plains material and densely ridged plains material often parallel tectonic lineations, suggesting topographic control. Superposes densely ridged plains materials and Nefertiti corona flows. Very low rms slope. *Interpretation*: Low radar backscatter coefficient suggests a very smooth surface texture at the cm scale, consistent with flooding by low-viscosity magma

pt **Intratessera plains material**—Low radar return, homogenous image texture; occurs in topographically confined regions of larger tessera outcrops. *Interpretation*: Smooth-surface lava flows that flood low-lying regions of tessera. Source vents and timing with respect to plains surrounding tessera materials indeterminate

prr **Ridged plains material**—Mottled to homogeneous image texture, with superposed E–W or SE–NW wrinkle ridges; backscatter varies with location from low to moderate radar return. *Interpretation*: Plains formed by volcanic flooding which have undergone varying degrees of tectonic deformation. Remote sensing data are consistent with moderate cm-scale roughness

prrd **Densely ridged plains material**—Radar backscatter properties variable due to the density of ridges, but background similar to ridged plains materials. High density of wrinkle ridges or fractures superposed on plains-forming material; contacts between these areas and ridged plains materials uncertain, but change in density of wrinkle ridges is significant. *Interpretation*: Regional plains formed by flood lavas, which have undergone tectonic deformation and emplacement of corona-like annular features. Age relationship to ridged plains materials indeterminate

prl **Densely lineated plains material**—Bright radar return, with mottled texture and typically single dominant lineament trend; forms parts of Nefertiti Corona rim deposits. *Interpretation*: Older plains materials which have been deformed by compression. May be transitional between ridged plains material and tessera material

TESSERA MATERIAL

t **Tessera material**—Radar bright regions elevated relative to surrounding plains; highly deformed in multiple directions by fractures, ridges, and graben; embayed by lobate materials or plains materials. Blocks which surround Tepev Mons are oriented along a SW–NE trend. *Interpretation*: Highly deformed terrain, presumably derived from older plains materials. Similarity of trends among many fragments suggests that they were at one time connected, and have since been largely covered by plains or edifice lava flows. Alternatively, these units may have undergone similar deformation due to regional stress patterns. Relative ages of isolated tessera outcrops indeterminate

IMPACT CRATER MATERIALS

cu **Crater material, undifferentiated**—Radar-bright material surrounding a central depression, rim materials, and floor materials of radar-bright and radar-dark varieties; exterior deposits typically lobate, with patchy radar image texture and bright streaks radial to the central cavity. *Interpretation*: Crater formed by impact onto the surface. Hummocky texture of near-rim material reflects distribution of continuous ejecta. Radar bright floors may be fractured impact melt, while radar-dark floors may reflect post-emplacement volcanic flooding or smooth impact melt

co **Crater outflow material**—Mottled or swirled radar image texture, with lobate margins and streaks parallel to the downhill direction; typically of moderate radar brightness, but can be as bright as the near-rim material. *Interpretation*: Melt generated by the impact event that escapes from the crater cavity to form a lava-like flow deposit. High radar brightness may be linked to enhanced reflectivity of melt rocks

Contact—Dashed where gradational or inferred

Graben

Radar-bright lineament

Wrinkle ridge—Schematic

Lobate scarp

Flow direction—Volcanic

Dome or shield
Diameter less than 20 km
Diameter greater than 20 km

Endogenic crater or caldera
Diameter from 10 to 20 km
Diameter greater than 20 km

Pit crater or chain of craters

Crater rim
Diameter less than 20 km
Diameter greater than 20 km

Central peak

Detached lobe—Interpreted as debris apron from southern edifice of Otafuku Tholi, likely formed by slope failure

Mantling material—Interpreted as fine-grained material that mantles underlying surface and reduces backscatter return

Caldera floor material—Interpreted as fine-grained deposit formed by surface-atmosphere interaction in calderas of Tepev Mons

The Magellan Mission

The Magellan spacecraft orbited Venus from August 10, 1990, until it plunged into the venusian atmosphere on October 12, 1994. Magellan had the objectives of (1) improving knowledge of the geologic processes, surface properties, and geologic history of Venus by analysis of surface radar characteristics, topography, and morphology and (2) improving knowledge of the geophysics of Venus by analysis of venusian gravity.

The Magellan spacecraft carried a 12.6-cm radar system to map the surface of Venus. The transmitter and receiver systems were used to collect three datasets: synthetic aperture radar (SAR) images of the surface, passive microwave thermal emission observations, and measurements of the backscattered power at small angles of incidence, which were processed to yield altimetric data. Radar imaging and altimetric and radiometric mapping of the venusian surface were done in mission cycles 1, 2, and 3, from September 1990 until September 1992. Ninety-eight percent of the surface was mapped with radar resolution of approximately 120 meters. The SAR observations were projected to a 75-m nominal horizontal resolution; these full-resolution data compose the image base used in geologic mapping. The primary polarization mode was horizontal-transmit, horizontal-receive (HH), but additional data for selected areas were collected for the vertical polarization sense. Incidence angles varied from about 20° to 45°.

High-resolution Doppler tracking of the spacecraft was done from September 1992 through October 1994 (mission cycles 4, 5, 6). High-resolution gravity observations from about 950 orbits were obtained between September 1992 and May 1993, while Magellan was in an elliptical orbit with a periapsis near 175 kilometers and an apoapsis near 8,000 kilometers. Observations from an additional 1,500 orbits were obtained following orbit-circularization in mid-1993. These data exist as a 75° by 75° harmonic field.

Magellan Radar Data

Radar backscatter power is determined by the morphology of the surface at a broad range of scales and by the intrinsic reflectivity, or dielectric constant, of the material. Topography at scales of several meters and larger can produce quasi-specular echoes, with the strength of the return greatest when the local surface is perpendicular to the incident beam. This type of scattering is most important at very small angles of incidence, because natural surfaces generally have few large tilted facets at high angles. The exception is in areas of steep slopes, such as ridges or rift zones, where favorably tilted terrain can produce very bright signatures in the radar image. For most other areas, diffuse echoes from roughness at scales comparable to the radar wavelength are responsible for variations in the SAR return. In either case, the echo strength is also modulated by the reflectivity of the surface material. The density of the upper few wavelengths of the surface can have a significant effect. Low-density layers, such as crater ejecta or volcanic ash, can absorb the incident energy and produce a lower observed echo. On Venus, a rapid increase in reflectivity exists at a certain critical elevation, above which high-dielectric minerals or coatings are thermodynamically stable. This effect leads to very bright SAR echoes from virtually all areas above that critical elevation.

The measurements of passive thermal emission from Venus, though of much lower spatial resolution than the SAR data, are more sensitive to changes in the dielectric constant of the surface than to roughness. As such, they can be used to augment studies of the surface and to discriminate between roughness and reflectivity effects. Observations of the near-nadir backscatter power, collected using a separate smaller antenna on the spacecraft, were modeled using the Hagfors expression for echoes from gently undulating surfaces to yield estimates of planetary radius, Fresnel reflectivity, and root-mean-square (rms) slope. The topography data produced by this technique have horizontal footprint sizes of about 10 km near periapsis and a vertical resolution of approximately 100 m. The Fresnel reflectivity data provide a comparison to the emissivity maps, and the rms slope parameter is an indicator of the surface tilts, which contribute to the quasi-specular scattering component.

INTRODUCTION

The Bell Regio quadrangle (V–9) of Venus is bounded by lat 25° and 50° N, long 30° and 60° E. This quadrangle is one of 62 covering Venus at the 1:5,000,000 scale. Bell Regio, named for an English giantess, is a broad rise, approximately 1,500 km in diameter, which is characterized by extensive effusive volcanism centered on five major sources: Tepev Mons [30° N., 45° E.], Nefertiti Corona [36° N., 48° E.], Nyx Mons [30° N., 48.5° E.], and two small, steep edifices on the southeast flank of Tepev named Otafuku Tholi [28.9° N., 46.1° E.; 28.6° N., 46.6° E.]. The shield volcano Api Mons [38° N., 55° E.] lies to the northeast of the central Bell highland (fig. 1). The summit of Tepev Mons reaches nearly 6 km elevation, and the edifices of Otafuku Tholi are 4–5 km above the planetary mean radius of 6051 km (fig. 2). Flank slopes on the large volcanoes vary widely. Api and Nyx Montes have typical slopes of only 1–2°, whereas the central massif of Tepev Mons has 20–40° flanks. The two edifices of Otafuku Tholi have slopes of up to 40° and are thus among the steepest large volcanic structures on the planet. The background terrain is largely smooth volcanic plains (Leda Planitia) bounded to the north, east, and south by Laima Tessera, Tellus Tessera, and western Aphrodite Terra. To the west lies several thousand kilometers of plains (Sedna Planitia, Guinevere Planitia), which end at the rift zones of Beta Regio. Elevations in these plains are typically about 1 km below the planetary mean radius, with the lowest central areas of Leda Planitia reaching 2 km below the datum. The quadrangle also includes numerous smaller outcrops of tessera surrounding Bell Regio.

Much of the early work on this region focused on characterizing the nature of isostatic compensation beneath Tepev Mons, concluding that some form of dynamic support (that is, a hotspot plume) is required to explain the gravity signature of this mountain. The geology and geophysics of the region were discussed by Janle and others (1987, 1988), but these analyses were hampered by the limited image coverage and a reliance on coarse-resolution Pioneer-Venus (PVO) altimeter data for gravity modeling. Smrekar and Phillips (1991) included Tepev Mons in a study of the gravity signatures of volcanic edifices, and more recent work (Stofan and others, 1995; Solomon and others, 1992; Senske and others, 1992; McGovern and Solomon, 1992) has used Magellan data to place Bell Regio within a global framework of large volcanic rises. Magellan circular-orbit gravity data have improved the estimates of crustal compensation for the region (Konopliv and others, 1993; Smrekar, 1994). Campbell and Rogers (1994) carried out a geologic study of the area which used Magellan radar/emission data and Venera images, and compared the results to radar data for Hawaiian lava flow surfaces to place the various units in a terrestrial context. Rogers and Zuber (1998) studied the distribution and formation of circumferential tectonic features surrounding the larger volcanoes and interpreted these data in terms of crustal thickness and possible magma chamber geometry.

Bell Regio is of considerable geologic interest as the site of effusive volcanic features which vary widely in elevation, flank slope, and surface morphology. Bell Regio is also distinct among large venusian highlands in having no associated rifting. This makes it possible to focus on the stratigraphic sequence of the volcanic materials and to assess possible changes in eruption style or magma rheology over time. Likewise, tectonic features on the individual volcanoes reflect primarily the stresses present during their formation. The stratigraphy developed in this study should provide important data for models of Venus highland evolution.

METHODS AND DATA USED

This geologic map was compiled from Magellan radar images at a base resolution of ~260 m/pixel; the map base was prepared from Magellan data by the U.S. Geological Survey. The full-resolution (75 m/pixel) U.S. Geological Survey F-MAP data were used to check unit contacts and to identify subtle or small features. Most of the quadrangle lies within the superior conjunction gap of the first Magellan mapping cycle, so the image data used here were collected primarily during cycle 2. These data have radar incidence angles of 32°–44°. Only a small part of the quadrangle was covered by Magellan cycle 3 stereo observations. Altimetry data were derived from both resampled topographic maps having 5.4 km horizontal resolution and from analysis of individual Magellan altimeter footprint records (Ford and Pettengill, 1992). Additional image data from the Venera 15/16 radar mapping missions were used to study the caldera region of Tepev Mons and the area surrounding Otafuku Tholi; these data cover gaps in the Magellan images and provide a lower radar incidence angle for comparison. Magellan emissivity, root-mean-square (rms) slope, and Fresnel reflectivity data provide valuable additional information on the presence and nature of surficial deposits.

Unit boundaries in the geologic map were defined primarily on the basis of changes in surface morphology and structure inferred from the radar data. The mapped units were placed within a tentative relative age sequence based on superposition and cross-cutting relations, shown in the accompanying correlation chart. Radar backscatter strength at the incidence angles used here is controlled largely by the wavelength-scale roughness of the surface. Changes in the backscatter coefficient of the surface due to variations in the bulk dielectric constant play a secondary role for most areas on Venus below ~6054 km radius unless there is a significant depth of fine-grained mantling material. Above this elevation, surface-atmosphere interactions produce highly reflective terrain for which roughness is a secondary factor in the backscattered return (Campbell, 1995). Near 6056 km radius, the surface no longer exhibits highly reflective behavior, and remote sensing evidence suggests that a fine-grained mantling layer develops above this elevation (Campbell and others, 1999). Magellan ancillary data on surface emissivity and reflectivity were used to further constrain surface unit properties.

STRATIGRAPHY

The stratigraphic units in the Bell Regio quadrangle have been grouped into six categories: tessera materials, plains materials, materials of central volcanoes, miscellaneous volcanic materials (which include corona-related flow fields and isolated shield volcanoes), impact crater materials, and surficial materials. Unit names are chosen to identify each unit by its primary properties or to show association with a major topographic feature. Quantitative backscatter and ancillary data for type areas of mapped units are presented in table 1, and the relative backscatter properties of selected major units are presented in a comparison with radar data for terrestrial lava flows in figure 3.

TESSERA MATERIAL

The oldest exposed unit in the quadrangle comprises complex ridged terrain, or tessera material (unit t). All tessera regions are embayed by plains units and (or) edifice lava flows. Large tessera blocks surround Bell Regio, and many are elongate in the SW–NE direction. The 700-km-long Adrasthea Tesserae, east of Nyx Mons, host fractures that are less regularly oriented than those associated with the western outcrop, Vako-nana Tesserae. The eastern part of Kruchina Tesserae lies along the west margin of the map area. The northern part of the map area is dominated by Laima Tessera, whose periphery has been embayed by plains-forming materials and whose enclosed upland regions have been partly buried by volcanic flow materials. Radar-dark wind streaks near the margins of some tessera are likely fine-grained material blown from higher-standing terrain through topographic gaps. It is not possible to determine the age of various tessera outcrops relative to one another, nor the absolute age of these units relative to any overlying materials. Though all appear to predate the plains and volcanic edifices, we cannot determine whether the extensively deformed tessera material formed concurrently or over an extended period of time.

PLAINS MATERIALS

The terrain surrounding Bell Regio is dominated by regional plains, whose materials we have subdivided into four units. All are interpreted to have originated as the result of extensive flooding by low-viscosity (for example, basaltic) volcanic material. Where not affected by tectonic deformation, their surfaces are quite smooth at both the hundreds of meter scale (as evidenced by their 1–2° rms slopes) and the centimeter scale (as shown by their low radar cross section: table 1, fig. 3). Radar image texture varies from homogeneous to swirled, streaked, or mottled patterns that may indicate the presence and aeolian movement of surficial fine materials. Few plains areas exhibit distinct lobate flow margins.

Outcrops of densely lineated plains material (unit prl) occur as small inliers along the east and west margins of the map area, typically in association with larger outcrops of tessera terrain. These lineated plains differ from tessera in having typically only one major set of ridges and appear to be areas of regional plains which have been highly deformed. We also have included the materials of the Nefertiti Corona rim in this classification. Densely lineated plains material (unit prl) has the highest rms slope (table 1) of the four regional plains units.

Most of the region surrounding Bell Regio comprises regional plains units we have designated as densely ridged plains material (unit prrd) and ridged plains material (unit prr). Material of unit prrd is characterized by a dense network of wrinkle ridges and numerous annular tectonic deformation patterns similar to coronae. The largest of these corona like features have linear fractures which trend radial or parallel to the uplifted and deformed annular ridged terrain. The ridged plains material (unit prr) has a much lower abundance of wrinkle ridges, typically consisting of a single major trend and a less distinct, variable background pattern. The densely ridged plains material has slightly higher average rms slope values than the ridged plains material (table 1). Contacts between densely ridged plains material and ridged plains material are poorly constrained, and our interpretation that the densely ridged plains are older is not supported by clear and extensive cross-cutting or embayment relations. The densely ridged plains material and the ridged plains material possibly formed contemporaneously, and the current difference in the abundance of lineaments and wrinkle ridges may reflect only spatial variations in subsequent tectonic deformation.

The youngest regional plains material (unit prs) occurs as patches of homogeneous low radar return that superpose the densely ridged and ridged plains materials (units prrd and prr). These smooth plains materials appear to flood older plains, subduing wrinkle ridge topography and reducing the centimeter-scale roughness of the surface. The edges of the smooth plains material are often polygonal, suggesting that relatively thin flow units ponded against topographic obstacles such as wrinkle ridges. Where smooth plains material approaches the edge of a tessera block, the densely ridged plains material is often visible as a narrow ring of higher-standing terrain around the tessera margin. The smooth plains material north of Tepev Mons superposes thinner portions and embays higher-standing parts of the lobate flows from Nefertiti Corona, indicating that plains formation continued through the period of flow emplacement by at least this source region. Smooth plains material has the lowest rms slope of any plains unit (<1°).

Intratessera plains material (unit pt) forms localized radar-dark patches in topographic depressions within tessera. Mostly found in Laima Tessera, intratessera plains material is mapped as a unit distinct from the regional plains only where there is no evident connection with the exterior flows (for example, a break in the tessera margin that is flooded by regional plains). The relative timing of these volcanic materials and the surrounding plains cannot be determined.

MATERIALS OF CENTRAL VOLCANOES

The earliest edifice-forming volcanism in Bell Regio occurred at Nyx Mons. This volcano is characterized by gentle flank slopes (typically <1°), a central bulge surrounded by a topographic moat and a wishbone pattern of ridges, and a conspicuous radial pattern of pit crater chains (fig. 4). Circumferential fractures occur to the east, south, and northwest of the central area. Three major lava flow complexes are associated with Nyx Mons. Lowest lobate material of Nyx Mons (unit fN$_1$) forms a moderate- to low-radar-return field of flows that superpose the ridged plains and embay the tesserae to the south, extending radially up to 600 km from the center of the edifice. Middle lobate material of Nyx Mons (unit fN$_2$) also forms a radar-dark field of flows which radiate from the center of Nyx Mons and extend up to 450 km, superposing the proximal portions of unit fN$_1$. The eastern outcrops of these flows are marked by isolated bright margins which may represent the transition of smooth, broad lava flows to rougher, more distinct lobate structures; these lobes also may be higher-standing, embayed flows of unit fN$_1$. The youngest lobate materials of Nyx Mons (unit fN$_3$) form a prominent aggregate of radar-bright flows to the south and southwest of Tepev Mons. Many of these flows trend radial to Nyx Mons, and some appear to have erupted from fissures concentric to the edifice. To the southeast of Tepev Mons, these bright flows are superposed on the earlier lobate materials of Nyx Mons (units fN$_1$ and fN$_2$).

Tepev Mons is a 300-km-diameter shield volcano with a complex summit area comprising overlapping digitate flows and two large (11 and 31 km diameter) circular features (fig. 5). The summit features are likely calderas, although topographic studies show that they are relatively shallow (Campbell and Rogers, 1994). There is a well-defined pattern of radar-bright fractures circumferential to the central peak of Tepev Mons, with a few smaller radial tectonic features. Collapse pits and pit crater chains occur near the summit, and some may have been vents for volcanic material. Interfingered radar-bright and radar-dark lobate materials of Tepev Mons (unit fT) form an apron 150–200 km in radius around the summit and likely erupted from the calderas or from nearby pit craters or fissures. Because there is no clear contact between these flows and the deposits of Nyx Mons, we cannot establish the relative age of lobate materials from these two volcanoes (units fN$_3$ and fT).

Two steep-sided volcanic edifices, Otafuku Tholi (4.4 km and 4.9 km in elevation above the datum), occur southeast of Tepev Mons (fig. 2). Activity centered on the northern construct produced radar-bright lobate material (unit fO) that is superposed on lobate materials of Tepev and Nyx Montes (units fN$_2$ and fT). Lobate material of Otafuku Tholi encircles the Tepev summit apron and embays portions of a tessera to the north. McGovern and Solomon (1992) suggested that these flows follow and infill a topographic moat formed by lithospheric loading, and topographic data do suggest such a depressed region north of Tepev Mons. The southern edifice is mapped with aid from Venera 15/16 data (Campbell and Rogers, 1994). The southwest margin of this edifice comprises a set of scarps and adjacent hummocky terrain, mapped as flow debris, that appear to have formed by collapse of the volcano flank. A second (31 km diameter) steep-sided dome is west of this feature and is partially buried by later flows. A region of mottled radar return, also mapped as flow debris, extends to the east of the southern edifice and superposes lobate materials of Nyx Mons. These materials are quite rough at scales of several hundred meters, with structures that are knobby in some locales and ridge like in others.

Api Mons is a low-relief shield volcano having a maximum elevation of about 1.5 km (fig. 4). Lobate materials of Api Mons (unit fA) are in general of low radar return, with well-developed lobate structure only in their distal portions. The summit area comprises a set of annular fractures or grabens with a few small pit craters. To the north, these flows embay outliers of Laima Tessera. On the northwestern flank of the edifice, Api Mons flows are diverted by the elevated rim of Heloise crater, which is in turn flooded by plains materials.

MISCELLANEOUS VOLCANIC MATERIALS

In the plains surrounding Bell Regio, localized lobate materials (unit fl) of moderate to bright radar return surround many low-relief shield volcanoes or caldera like depressions. Nefertiti Corona is surrounded by an apron of low to moderate radar return lobate material (unit fNe) which floods its interior and overlies parts of the rim deposits, extending ~100 km from the rim. Flows from Nefertiti are diverted eastward by an east-west trending region of higher topography just north of the corona.

IMPACT CRATER MATERIALS

A total of 13 impact craters occur in the Bell Regio quadrangle, and we have identified an additional 12-km circular feature (Shirley) in Adrasthea Tesserae (31.44° N., 55.44° E.) which may be a plains-flooded crater. The crater Conway (48.4° N., 39.1° E.) in Laima Tessera is distinguished by a crescent-shaped region of rough terrain along the north half of a roughly circular flooded depression. Though all of these craters are younger than the tessera units, several (for example, Gautier and Heloise) are embayed by materials of plains or central volcanoes. We have divided the impact crater materials into two broad categories: undifferentiated material of crater rims, floors, and ejecta blankets (unit cu), and crater outflow material (unit co). Crater floors vary in radar return from very bright (for example, Miriam) to dark (for example, Potanina). The bright floors are likely rough due to emplacement of a fractured impact melt sheet, whereas the dark floors may reflect post-excavation flooding by volcanic materials or a smooth melt sheet. The outflow deposits mapped in association with Potanina, Voynich, and Liliya are common to Venus craters and likely form as a result of impact melt ejection from the central cavity. These melt deposits are characterized by low to high radar return, with swirled interior texture and lobate margins. The large outflow deposit associated with Potanina has interior digitate flow margins.

SURFICIAL MATERIALS

Surficial deposits in the Bell Regio quadrangle are predominantly of impact origin, and represent thin (on the order of 10–50 cm) layers of fine-grained material which reduce the radar echo by smoothing the surface and lowering the effective reflectivity. Analysis of the Magellan emissivity data (fig. 6) and altimeter-derived reflectivity and rms slope estimates for surficial materials provides important information on their roughness and dielectric properties (Campbell and Rogers, 1994; Campbell, 1994).

The region surrounded by the craters Miriam, Potanina, Voynich, and Aisha is characterized by large feathery-edged areas of low radar return and numerous radar-dark wind streaks or "shadows" along the edges of topographic obstacles. We interpret these radar-dark areas to be deposits of fine-grained mantling material produced by impact events and reworked by either the prevailing winds or those of later impacts. The presence of this material obscures the contacts between flows from Nefertiti Corona and Nyx Mons and the regional plains. A halo of smooth material with lower emissivity than the plains (estimated real dielectric constant of 6–7) surrounds Nefertiti Corona and also is associated with Miriam crater (fig. 6). This deposit forms a roughly parabolic shape open to the west, similar to the low-emissivity crater parabolas studied by Campbell and others (1992). The interior of the parabola is radar-bright relative to the surrounding plains, suggesting either a layer of clastic debris or the removal of pre-existing fine material from this area. The parabola itself is not easily discerned in backscatter images, implying that the deposit is quite thin. The ejecta which forms the parabola must therefore contain materials with high permittivity to offset the normal decrease in dielectric constant with lower density (Ulaby and others, 1988). The occurrence of high-dielectric materials in crater ejecta may be due to impact melting and recondensation of the target rock (Schultz, 1992; Campbell, 1994).

A roughly triangular area of low radar backscatter with feathery margins, mapped as fine-grained mantling material, occurs just south of the summit of Tepev Mons and widens toward the west. This dark material appears to completely blanket upper lobate materials of Nyx Mons (unit fN$_3$) at the northeast apex of the triangle, and thins out to expose more of the underlying materials as the deposit widens. There is no associated crater like feature or bright central region. Emissivity data suggest that the dielectric constant of this material is low (2–3), consistent with a porous mantling layer. The lack of an obvious central crater leaves open the possibility of a pyroclastic origin for this feature; alternatively, this may be an impact "splotch".

The Tepev Mons calderas are close to the upper transitional elevation (~6056 km radius) at which highly reflective surfaces no longer occur (Arvidson and others, 1994), and remote sensing data for high-elevation areas in Ovda Regio and elsewhere suggest that fine-grained mantling deposits are present in these areas (Campbell and others, 1999). Analysis of Magellan and Venera data by Campbell and Rogers (1994) shows that the eastern Tepev Mons caldera floor also may be covered by a fine-grained deposit. The mode of formation of such a layer is unknown, but is unlikely to be related to impact crater processes. The caldera floors are thus mapped to show a separate surficial material.

The high-dielectric (low emissivity) areas between about 6054 km and 6056 km in radius are not mapped as a separate surficial unit, because at the map scale they are almost entirely elevation dependent and they do not appear to define distinct rock unit boundaries. The dielectric constant over the Tepev Mons summit reaches a maximum value of 35, well in excess of typical dense basaltic rock. The areas of highest dielectric constant are near the western caldera.

STRUCTURE

RIDGES IN THE PLAINS

The plains surrounding Bell Regio host a complex array of apparently compressional ridge structures, which can be used as a constraint on the history of the region. Northwest of Bell Regio, both densely ridged (unit prrd) and ridged (unit prr) plains materials have southwest-northeast trending ridges with similar horizontal spacing. In the densely ridged plains, the orientation of these ridges shifts in the vicinity of corona like deformation patterns, assuming a roughly radial pattern about the larger structures. North of Bell Regio, the plains structures trend generally north-south, with some small ridges paralleling the margins of an east-west elevated strip of densely ridged plains just north of Nefertiti Corona.

A background fabric of more closely spaced, possibly lower-relief ridges occurs between the brighter, more distinct southwest-northeast lineaments. This background fabric in some areas parallels the major structures, and in other locales forms a nearly orthogonal, grid like pattern. In the ridged plains (unit prr), this pattern appears to be superposed to varying degrees by radar-dark homogenous material. No distinct lobate margins or obvious embayments exist at the map base scale, but the ridged plains material apparently superposes the pre-existing densely ridged plains. The major southwest-northeast trending ridges are thus inferred to be high-standing remnants of densely ridged (unit prrd) structures.

EDIFICE GRABENS AND FRACTURES

The two large volcanoes in Bell Regio, Tepev and Nyx Montes, have tectonic deformation patterns which may be used to infer the thickness of the supporting crust at the time these edifices formed. The dominant tectonic features on both volcanoes are circumferential radar-bright arcuate lineaments and grabens, interpreted to be the result of extension due to lithospheric flexure or edifice stresses. A similar set of concentric radar-bright lineaments are associated with the north flank of the northern edifice of Otafuku Tholi. These features are mapped in detail in figure 7.

Rogers and Zuber (1998) analyzed these extensional deformation features using an analytical model for an elastic lithosphere of unknown thickness and a finite-element model of edifice stresses resulting from the inflation of a subsurface magma reservoir. The analytical model shows that the annular fractures surrounding Nyx Mons are well modeled by an elastic lithosphere approximately 50 km thick, consistent with values for large spatial wavelengths obtained from gravity data analysis by Smrekar (1994). A similar elastic lithospheric thickness is consistent with the location of the postulated topographic moat north of Tepev Mons, marked by the radar-bright lobate flows of unit fO. The tectonic fractures surrounding Tepev Mons are not well modeled by lithospheric flexure, and Rogers and Zuber (1998) proposed that these features formed as a result of stresses induced in the edifice by an inflating magma chamber. Though results for the size and shape of such a chamber are nonunique, finite-element modeling suggests that a horizontally ellipsoidal chamber at a depth of 20-40 km could produce the observed deformation pattern.

CORONAE

Nefertiti is the largest corona in Bell Regio (500 km by 230 km in diameter), with a central depression surrounded by broad topographic highs. The initial uplift of Nefertiti may have produced a roughly circular feature, but the eastern parts of the rim have been deformed ~200 km toward the east-southeast, creating an oblong appearance and widespread short linear fractures. Nefertiti is also the source of a major lobate flow complex that has buried portions of the corona rim and superposes the surrounding ridged plains. Branwen Corona (27° N., 34.5, E.), 160 km in diameter, lies west of Tepev Mons; bounding structures are characterized by elevated central topography and parallel exterior depressions, consistent with coronae mapped elsewhere on Venus (Stofan and others, 1992). Volcanism at this site is confined to radar-dark plains material within the arcuate deformed rims. Kayanu-Hime Corona, near the crater Potanina, is typical of concentric tectonic deformation patterns across the quadrangle. These features are characterized by annular radar-bright arcuate lineaments, in some cases accompanied by radial lineaments. Typically on the order of a few tens of kilometers in diameter, they lack associated deformed rim terrain and lobate flow materials.

GEOLOGIC SUMMARY

The geologic history of the area surrounding Bell Regio may be reconstructed from superposition, embayment, and cross-cutting relations among the mapped units and structures. What remains uncertain are the absolute time scales over which various processes occurred, and the distribution of ages among separated outcrops of similar units (for example, tessera) across the mapped region. Though this quadrangle contains a number of impact craters, and some display clear evidence of burial or embayment by later volcanic materials, no statistical analysis of their locations or frequency can yield meaningful results. We thus describe the progression of geologic events within the region without proposing a relative or absolute timescale.

Tessera appears to be the oldest exposed material within the quadrangle. The presence of tessera blocks with similar deformation patterns surrounding Bell Regio may indicate that the mantle plume which supplied the magma for subsequent eruptions impinged on the base of a large tessera region and subsequently buried much of it. The nature of the material from which tessera units formed is also not evident, though regional plains deposits seem the most plausible original terrain. Plains-forming volcanism, likely in the form of high-volume, low-viscosity flood lavas, occurred after the emplacement and deformation of tessera terrain. The bulk of the plains in this quadrangle are divided provisionally into two units, though their differences lie primarily in the density of wrinkle ridges and the presence of annular deformation patterns similar to coronae. The more densely ridged terrain, with its population of corona like features, likely predates the less ridged plains, but these areas may simply record preferential deformation patterns in essentially contemporaneous background material.

The Bell Regio central uplift probably followed plains emplacement. The superposition and embayment of Nefertiti lava flows by smooth plains material (unit prs), however, indicates that plains-forming events continued at least beyond the period during which this corona was volcanically active. Coronae may have been a dominant feature of the early highland, as evidenced by the remnants of Nefertiti to the north and the central wishbone-shaped structure of Nyx Mons. This scenario (plains followed by coronae followed by central volcanoes) is consistent with that found by McGill (1994, 1998) in Eistla Regio. The relative contributions of constructional volcanism and plume-driven uplift cannot be established. No evidence exists for a major rift zone at any time during the formation of Bell Regio, which distinguishes this highland from western Eistla, Atla, and Beta Regiones, all of which have volcanism connected with extensive rifting.

Impact craters in this quadrangle have relative ages that straddle the formation of the regional plains and the development of large volcanic edifices. Fine-grained debris produced by these craters is reworked by the prevailing winds or those from later impacts, creating local concentrations of mantling layers. These surficial deposits and those found at high elevations have dielectric properties that vary with the local temperature/pressure regime and possibly age.

The stratigraphically youngest materials of Bell Regio are dominated by effusive volcanic deposits from Tepev and Nyx Montes, Otafuku Tholi, and Nefertiti Corona. Flows from Api Mons form a distinct low shield in the nearby plains. The surface morphology and planform shape of these flows vary among the major source regions, and the edifices are characterized by widely differing elevations and flank slopes. Flank sources for magma at the large volcanoes appear to be primarily pit craters, calderas, or arcuate fissures. Little evidence exists for smaller parasitic shields on either Nyx or Tepev Mons. The relatively oldest flows are associated with Nyx Mons, whose central deposits have very low radar returns consistent with a smooth surface at the centimeter scale (table 1, fig. 3). Flank slopes on Nyx Mons are very gentle (on the order of 1–2°). The lava flows of Tepev Mons likely postdate at least the earlier flows of Nyx Mons, and the edifice is characterized by steep sides and large summit calderas. Tepev Mons lava flows are also shorter and narrower than those of Nyx Mons. The two volcanoes that form Otafuku Tholi resemble steep-sided volcanic constructs found in some plains regions of Venus, but are considerably taller (4–5 km above the datum). Lava flows associated with these volcanoes are radar bright, and the largest discrete lobate deposit has a radar-dark central channel structure consistent with terrestrial aa flows (Campbell and Rogers, 1994).

The progression toward rougher flow surface morphology and steeper edifice flank slope with decreasing relative age suggests that the magma supplied to these volcanoes may have become more viscous (higher silica content) over time. Geophysical analyses indicate that Nyx Mons likely formed over a thinner elastic lithosphere than that which hosted the Tepev Mons magma chamber. Thus the changes in volcanic style with time as mapped here correspond to a thickening of the local lithosphere between the period of the earliest mapped Nyx Mons flows and the deposits of Otafuku Tholi. A thickening lithosphere would inhibit rising magma bodies from directly erupting onto the surface and promote the development of crustal magma chambers. These chambers might have permitted the production of more evolved magma to create the rough lava flows and steep edifices.

Acknowledgments—This work was funded in part by grants from the Venus Data Analysis Program and the NASA Planetary Geology and Geophysics Program (NAGW-3360). The authors thank J. Zimbelman for helpful discussions, and K. Bender, R. Greeley, G. McGill, E. Stofan, and K. Tanaka for constructive reviews.

REFERENCES CITED

Arvidson, R.E., Brackett, R.A., Shepard, M.K., Izenberg, N.R., Fegley, B., and Plaut, J.J., 1994, Microwave signatures and surface properties of Ovda Regio and surroundings, Venus: Icarus, v. 112, p. 171–186.
Campbell, B.A., 1994, Merging Magellan emissivity and SAR data for analysis of Venus surface dielectric properties: Icarus, v. 112, p. 187–203.
———1995, Use and presentation of Magellan quantitative data in Venus mapping: U.S. Geological Survey Open-File Report 95–519, 32 p.
Campbell, B.A., Campbell, D.B., and DeVries, C., 1999, Surface processes in the Venus highlands: Results from analysis of Magellan and Arecibo data, Journal of Geophysical Research, v. 104, p. 1897–1916.
Campbell, B.A., and Rogers, P.G., 1994, Bell Regio, Venus: Integration of remote sensing data and terrestrial analogs for geologic analysis: Journal of Geophysical Research, v. 99, p. 21,153–21,171.
Campbell, D.B., Stacy, N.J.S., Newman, W.I., Arvidson, R.E., Jones, E.M., Musser, G.S., Roper, A.Y., and Schaller, C., 1992, Magellan observations of extended impact crater related features on the surface of Venus: Journal of Geophysical Research, v. 97, p. 16,249–16,278.
Ford, P.G., and Pettengill, G.H., 1992, Venus topography and kilometer-scale slopes, Journal of Geophysical Research, v. 97, p. 13,103–13,114.
Janle, P., Jannsen, D., and Basilevsky, A.T., 1987, Morphologic and gravimetric investigations of Bell and Eisila Regiones on Venus: Earth, Moon, and Planets, v. 39, p. 251–273.
———1988, Tepev Mons on Venus: Morphology and elastic bending models: Earth, Moon, and Planets, v. 41, p. 127–139.
Konopliv, A.S., Borderies, N.J., Chodas, P.W., Christensen, E.J., Sjogren, W.L., Williams, B.G., Balmino, G., and Parriot, J.P., 1993, Venus gravity and topography: 60th degree and order model: Geophysical Research Letters, v. 20, p. 2403–2406.
McGill, G.E., 1994, Hotspot evolution and venusian tectonic style, Journal of Geophysical Research, v. 99, p. 23,149–23,162.
———1998, Central Eistla Regio: Origin and relative age of topographic rise, Journal of Geophysical Research, v. 103, p. 5889–5896.
McGovern, P.J., and Solomon, S.C., 1992, Estimates of elastic plate thickness beneath large volcanoes on Venus, International Colloquium on Venus, Lunar and Planetary Institute Contribution 789, p. 68–70.
Pettengill, G.H., Ford, P.G., and Wilt, R.J., 1992, Venus surface radiothermal emission as observed by Magellan: Journal of Geophysical Research, v. 97, p. 13091–13102.
Rogers, P.G., and Zuber, M.T., 1998, Tectonic evolution of Bell Regio, Venus: Regional stres, lithospheric flexure, and edifice stresses, Journal of Geophysical Research, v. 103, 16,841–16,853.
Schultz, P.H., 1992, Atmospheric effects on ejecta emplacement and crater formation on Venus from Magellan: Journal of Geophysical Research, v. 97, p. 16,183–16,248.
Senske, D.A., Schaber, G.G., and Stofan, E.R., 1992, Regional topographic rises on Venus: Geology of Western Eistla Regio and comparison to Beta Regio and Atla Regio: Journal of Geophysical Research, v. 97, p. 13,395–13,420.
Smrekar, S.E., 1994, Evidence for active hotspots on Venus from analysis of Magellan gravity data, Icarus, v. 112, p. 2–26.
Smrekar, S.E., and Phillips, R.J., 1991, Venusian highlands: Geoid to topography ratios and their implications: Earth and Planetary Science Letters, v. 107, p. 582–597.
Solomon, S.C., Smrekar, S.E., Bindschadler, D.L., Grimm, R.E., Kaula, W.M., McGill, G.E., Phillips, R.J., Saunders, R.S., Schubert, G., Squyres, S.W., and Stofan, E.R., 1992, Venus tectonics: An overview of Magellan observations: Journal of Geophysical Research, v. 97, p. 13,199–13,256.
Stofan, E.R., Smrekar, S.E., Bindschadler, D.L., and Senske, D.A., 1995, Large topographic rises on Venus: Implications for mantle upwelling, Journal of Geophysical Research, v. 100, p. 23,317–23,328.
Stofan, E.R., Sharpton, V.L., Schubert, G., Baer, G., Bindschadler, D.L., Janes, D.M., and Squyres, S.W., 1992, Global distribution and characteristics of coronae and related features on Venus: Implications for origin and relation to mantle processes: Journal of Geophysical Research, v. 97, p. 13,347–13,378.
Ulaby, F.T., Bengal, T., East, J., Dobson, M.C., Garvin, J., and Evans, D., 1988, Microwave dielectric spectrum of rocks: University of Michigan Radiation Lab Report 23817–1–TU.

Table 1. *Physical properties of mapped units*

The first table presents information on type location, number of pixels (C1–MIDR, 225 m scale) used in the backscatter calculation (N), incidence angle, and radius. The second table lists backscatter coefficient $\sigma°$, RMS slope, Fresnel reflectivity, emissivity, and calculated dielectric constants for the smooth-surface (ε_s) and rough-surface (ε_r) cases (Campbell, 1995). Values in parentheses represent the minimum and maximum values of each parameter within the chosen sample box. Units whose properties vary significantly are noted with a low-backscatter (l) and high-backscatter (h) sample area. Some mapped units have been omitted where the microwave properties could not be meaningfully presented as a single value or range (for example, crater ejecta).

Unit	Type Location	N	Angle (deg)	Radius (km)
t	32.247–32.755 N; 44.329–44.691 E	34080	41	6052.208 (6051.577, 6052.614)
prs	29.526–29.623 N; 40.928–40.999 E	1470	42	6051.205 (6051.169, 6051.229)
prr	24.535–24.874 N; 41.188–41.794 E	40800	44	6051.220 (6051.115, 6051.264)
prrd	33.630–34.581 N; 35.777–36.604 E	145152	40	6051.264 (6050.692, 6051.664)
prl	36.861–37.029 N; 46.910–47.078 E	5120	39	6052.830 (6052.699, 6052.942)
fN$_1$	26.291–26.672 N; 50.300–51.458 E	86400	43	6051.949 (6051.833, 6052.090)
fN$_2$	29.128–29.682 N; 50.702–51.898 E	124497	42	6053.287 (6052.895, 6053.652)
fN$_3$ (h)	26.068–26.672 N; 47.862–48.433 E	66975	43	6051.521 (6051.315, 6051.723)
fN$_3$ (l)	27.089–27.426 N; 45.726–46.283 E	37047	43	6051.936 (6051.603, 6052.419)
fT	29.786–30.252 N; 46.002–46.565 E	50380	42	6052.022 (6051.432, 6052.367)
fA	37.859–38.550 N; 53.443–54.490 E	125510	39	6052.087 (6051.856, 6052.702)
fNe	37.321–37.557 N; 49.152–50.019 E	35728	39	6052.783 (6052.590, 6053.040)
fO (h)	30.561–30.646 N; 44.129–44.318 E	3157	42	6051.403 (6051.263, 6051.482)
fO (l)	29.130–29.390 N; 46.710–47.020 E	16104	42	6052.514 (6052.374, 6052.799)
Mantling material	28.475–28.658 N; 45.101–45.315 E	7743	43	6052.016 (6051.657, 6052.332)
Caldera floor material	29.505–29.678 N; 45.467–45.668 E	6806	42	6056.616 (6055.662, 6056.917)

Unit	$\sigma°$ (dB)	RMS Slope (deg)	Fresnel Reflectivity	Emissivity	ε_s, ε_r
t	–10.4	6.5 (2.4, 10.3)	0.079 (0.055, 0.105)	0.851 (0.817, 0.862)	3.3, 4.9
prs	–21.3	0.8 (0.5, 0.9)	0.127 (0.110, 0.145)	0.844 (0.841, 0.875)	3.4, 5.1
prr	–20.0	1.0 (0.5, 1.9)	0.099 (0.065, 0.135)	0.856 (0.851, 0.862)	3.1, 4.7
prrd	–16.4	2.4 (1.0, 4.8)	0.095 (0.075, 0.130)	0.857 (0.846, 0.875)	3.3, 4.7
prl	–8.8	2.9 (1.9, 3.4)	0.116 (0.100, 0.195)	0.835 (0.824, 0.839)	3.8, 5.5
fN$_1$	–17.5	0.8 (0.4, 1.3)	0.106 (0.070, 0.190)	0.843 (0.836, 0.850)	3.3, 5.1
fN$_2$	–21.1	1.7 (1.0, 2.7)	0.099 (0.075, 0.125)	0.852 (0.842, 0.862)	3.2, 4.8
fN$_3$ (h)	–10.6	3.5 (1.1, 6.8)	0.098 (0.075, 0.115)	0.814 (0.786, 0.863)	3.8, 6.1
fN$_3$ (l)	–12.2	3.3 (2.6, 4.0)	0.100 (0.090, 0.115)	0.832 (0.814, 0.846)	3.5, 5.4
fT	–13.6	4.3 (1.8, 8.7)	0.129 (0.045, 0.185)	0.849 (0.802, 0.865)	3.3, 4.9
fA	–19.4	1.9 (0.7, 3.4)	0.129 (0.100, 0.195)	0.838 (0.831, 0.846)	3.8, 5.4
fNe	–18.1	2.0 (1.2, 2.7)	0.160 (0.110, 0.200)	0.776 (0.748, 0.807)	5.1, 7.7
fO (h)	–8.2	8.5 (7.2, 9.9)	0.127 (0.095, 0.165)	0.871 (0.860, 0.882)	3.0, 4.0
fO (l)	–10.5	5.6 (2.5, 9.5)	0.146 (0.095, 0.250)	0.844 (0.832, 0.859)	3.3, 5.1
Mantling material	–24.2	1.3 (0.8, 3.3)	0.048 (0.040, 0.080)	0.926 (0.892, 0.940)	2.1, 2.8
Caldera floor material	–11.5	7.5 (3.9, 9.0)	0.122 (0.060, 0.195)	0.710 (0.637, 0.781)	6.6, 11.0

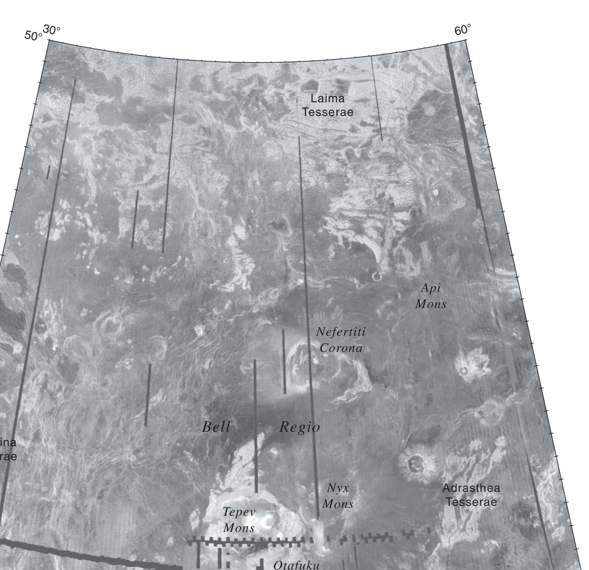

Figure 1. Synthetic aperture radar backscatter mosaic of Bell Regio quadrangle (V–9), showing nomenclature of major structures.

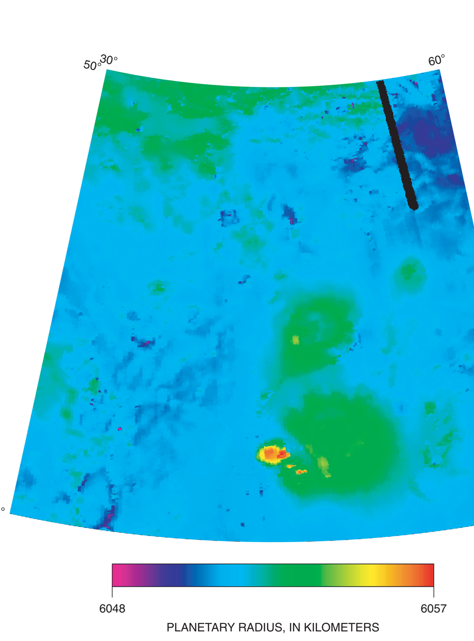

Figure 2. Topographic map of Bell Regio quadrangle (V–9), Venus.

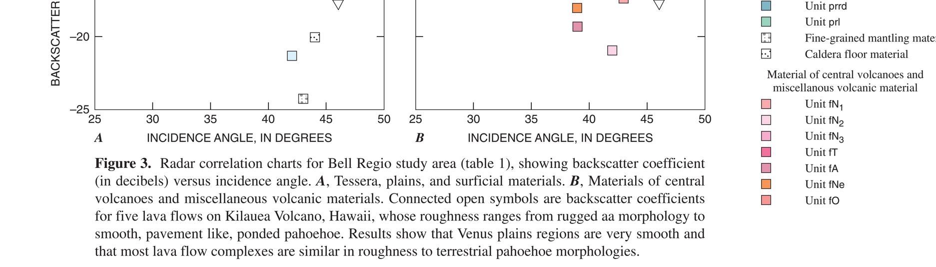

Figure 3. Radar correlation charts for Bell Regio study area (table 1), showing backscatter coefficient (in decibels) versus incidence angle. ***A***, Tessera, plains, and surficial materials. ***B***, Materials of central volcanoes and miscellaneous volcanic materials. Connected open symbols are backscatter coefficients for five lava flows on Kilauea Volcano, Hawaii, whose roughness ranges from rugged aa morphology to smooth, pavement like, ponded pahoehoe. Results show that Venus plains regions are very smooth and that most lava flow complexes are similar in roughness to terrestrial pahoehoe morphologies.

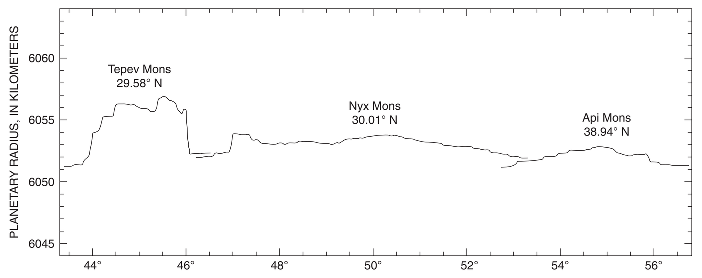

Figure 4. Topographic profiles through Tepev, Nyx, and Api Montes. Elevations are shown in terms of planetary radius. Profiles are east-west in orientation, with latitude marked above each transect.

Figure 5. Magellan SAR image of the Tepev Mons summit area (lat 27.6–31.9° N., long 42.0–47.6° E.). The two edifices that comprise Otafuku Tholi are at lower right.

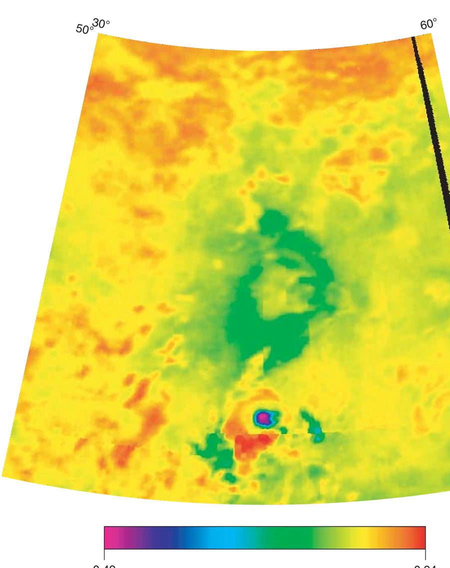

Figure 6. Map of Magellan emissivity data for Bell Regio quadrangle (V–9). Note high emissivity (low dielectric constant) region on south flank of Tepev Mons and low emissivity (increased dielectric constant) associated with parabolic ejecta deposit of Miriam crater. Areas between ~6054–6056 km have very low emissivity (very high dielectric constant) due to surface-atmosphere interaction.

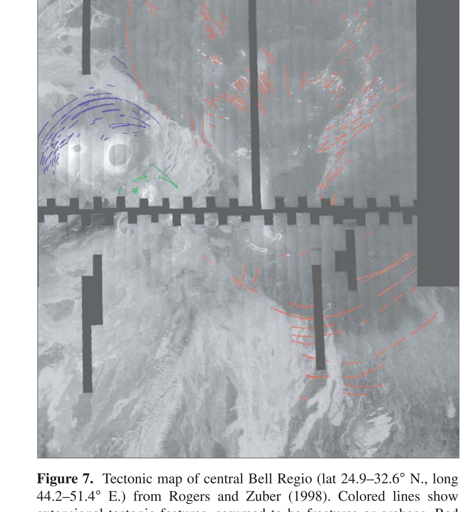

Figure 7. Tectonic map of central Bell Regio (lat 24.9–32.6° N., long 44.2–51.4° E.) from Rogers and Zuber (1998). Colored lines show extensional tectonic features, assumed to be fractures or grabens. Red lines are features associated with Nyx Mons, green lines with Otafuku Tholi, and blue lines with Tepev Mons.

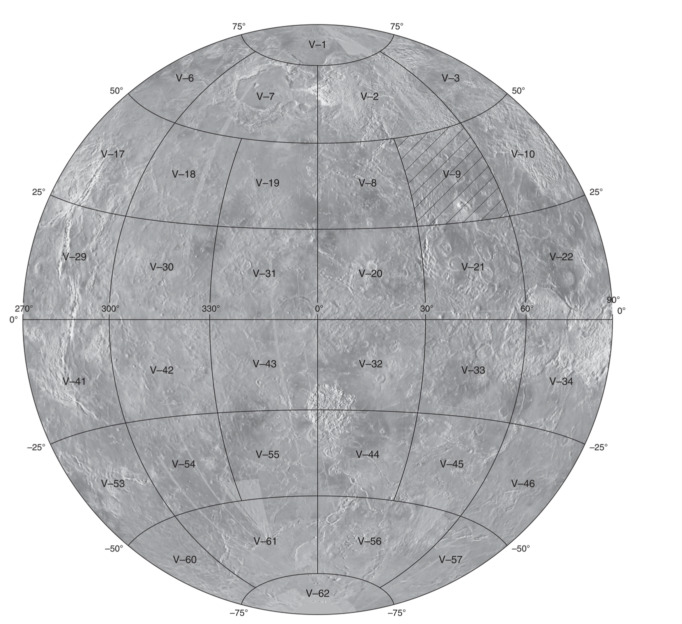

QUADRANGLE LOCATION
Photomosaic showing location of map area. An outline of 1:5,000,000-scale quadrangles is provided for reference.

GEOLOGIC MAP OF THE BELL REGIO QUADRANGLE (V–9), VENUS

By
Bruce A. Campbell and Patricia G. Campbell
2002

For sale by U.S. Geological Survey, Information Services, Box 25286, Federal Center, Denver, CO 80225, 1–888–ASK–USGS

ISBN 0-607-97508-3

Printed on recycled paper

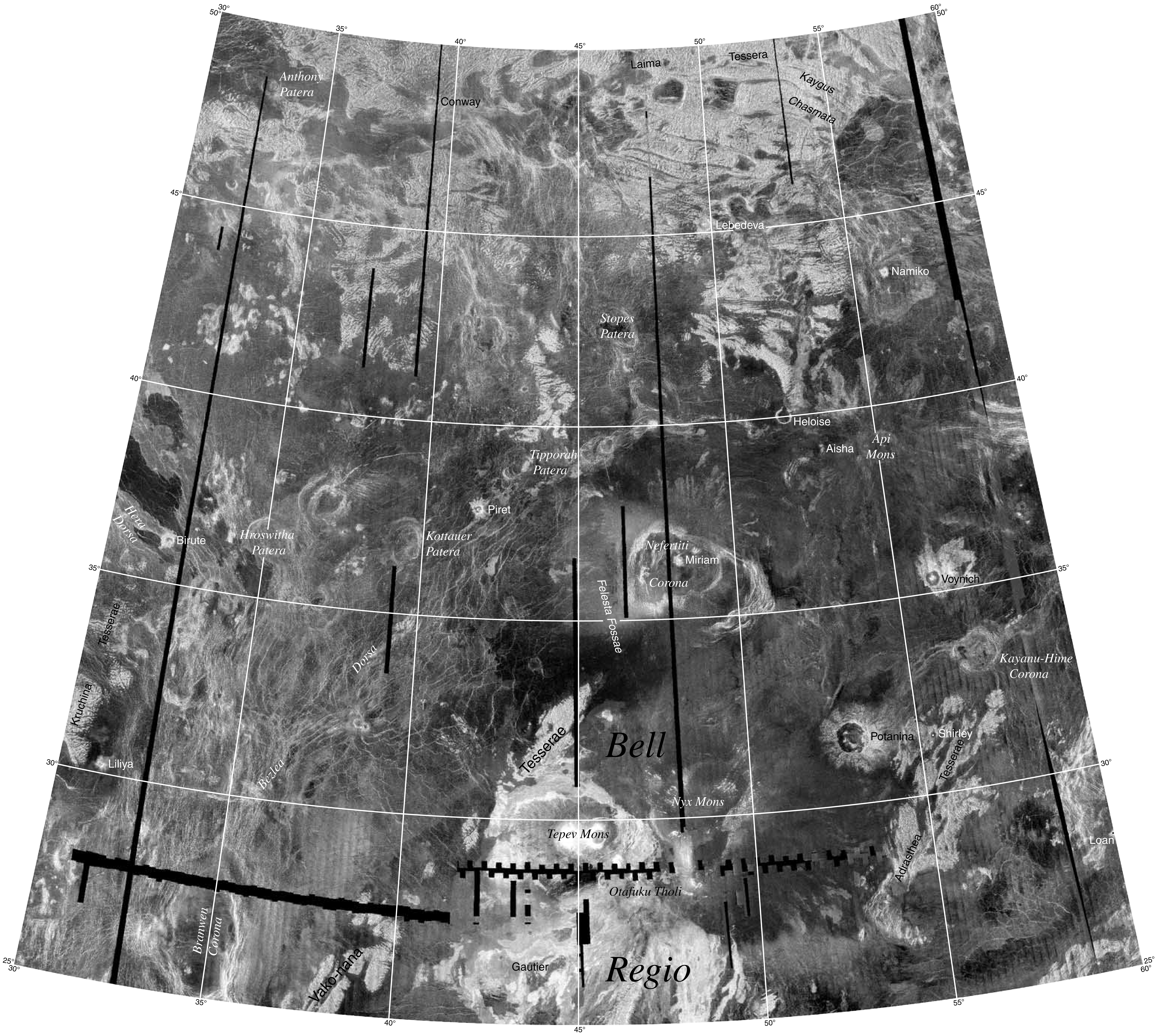

Anthony Patera
Conway
Laima
Tessera
Kaygus Chasmata
Lebedeva
Namiko
Stopes Patera
Heloise
Aisha
Api Mons
Tipporah Patera
Piret
Hera Dorsa
Birute
Hroswitha Patera
Kottauer Patera
Nefertiti Corona
Miriam
Voynich
Felesta Fossae
Tesserae
Dorsa
Kayanu-Hime Corona
Kruchina
Potanina
Shirley
Tesserae
Bell
Liliya
Bez-Lea
Nyx Mons
Tepev Mons
Adrasthea
Loan
Otafuku Tholi
Branwen Corona
Gautier
Regio
Vako-nana